Progress In Electromagnetics Research C, Vol. 99, 179–191, 2020

Design of Sub-THz Beam Scanning Antenna Using Luneburg Lens for 5G Communications or Beyond

Thevaruparambil A. Nisamol*, Kunnath K. Ansha, and Parambil Abdulla

Abstract—This work presents the design and simulation of a beam scanning antenna at 300 GHz using Luneburg lens for 5th generation communication applications or beyond. The basic antenna consists of a highly directional Yagi-Uda antenna with lens shaped configuration (substrate lens antenna-SLA) and designed using multiple parallel elements such as one reflector and one driven element with 6 directors. The SLA is focused by Luneburg lens, which is modeled using a unique foam material AirexR82 with relative dielectric constant of 1.12, and it is pressed to realize different dielectric constants in order to obey the index law inside the lens. The final nine-element array of SLA integrated with Luneburg lens provides a 50% increase in bandwidth compared with conventional Yagi-Uda antenna along with an increase in the gain of 31.3% compared with single SLA. The designed model can achieve a beam scan coverage up to 146° with a maximum gain of 17.1 dBi and an estimated efficiency of 92.9%. The beam scanning antenna provides a wide bandwidth of 83 GHz starting from 289 GHz to 372 GHz. The analysis of the proposed antenna is done in CST suite and is validated using HFSS software.

1. INTRODUCTION

The evolution of the ultra-fast mobile communication systems during the last few decades increases the demand of THz and sub-THz millimeter wave antennas. The design and development of antenna units are transformed beyond the fifth-generation wireless communication bands [1]. For the transmission of signals, researchers are searching for THz and sub-THz frequency bands (0.1 THz–10 THz), since very high data rates within the confined duration are becoming the major goal in the emerging communication field. In the past 20 years, NASA has been leading Terahertz (THz) technology development for the sensors and instruments in astronomy. THz technologies are expanding into much broader applications in recent years. Moreover, the emerging THz antennas extend their imaging technique towards the screening of metals, weapons, explosives in the military application [2]. Full duplex system which suppresses self interference is required for wide-band communication networks. Dual polarized antennas can be used with the full-isolation and SI reduction at 300 GHz [3]. However, the properties of higher losses at THz frequency than the losses observed at antennas working in lower frequency band below 0.1 THz limit the complete reduction of SI and isolation.

The design and criteria to enhance the gain and bandwidth of the antennas at higher frequencies are detailed in [4]. For the bandwidth extension and reduction in the reflection losses, the novel technologies in the field of reflect array antennas at 300 GHz were developed in [5, 6]. Since it is hard to limit the reflections around the high frequency resonances, there will be poor reflection loss characteristics at 300 GHz. While dealing with the recent developments in this band, the measurement setup with maximum accuracy of reflection losses is required. Some of the measurement techniques at sub-THz frequency bands were discussed in [7, 8]. The works advancing in THz frequency [9, 10] range also have high significance for the future communication applications.

Received 11 December 2019, Accepted 22 January 2020, Scheduled 7 February 2020
* Corresponding author: Thevaruparambil Abdulnazer Nisamol (nisamolshiyas2018@cusat.ac.in).
The authors are with Division of Electronics, Cochin University of Science and Technology, India.

The high gain antennas acquire more significance in high frequency applications. Highly directional printed Yagi-Uda antenna is the most common directive antenna which can achieve high gain and directivity using linear dipole elements such as reflector, directors, and feeding element. These kinds of antennas serve high data rates applications such as WIFI, WIMAX, and WLAN technologies. They are widely used to obtain broad bandwidth for communication applications, and most of the works are carried out on low frequency bands in the past years whose various wireless areas are already occupied with low data rates.

A planar Yagi-Uda antenna was used to provide high directivity to reduce free space path loss [11] and achieve better impedance matching when it was integrated with other circuits [12]. At lower frequencies, the bandwidth can be enhanced by varying the length and width of directors of the Yagi-Uda antenna which makes it suitable for RFID communication systems [13, 14]. A highly directional Yagi antenna at 193.5 THz was developed in [15] using modern techniques, particularly nano-photonics circuits and photovoltaic devices. The antenna developed in nano wavelengths is termed as nantenna which provides directivity of 16.6 dBi. Also, Yagi-Uda antenna gain possesses higher significance, and by focusing the power transmitted into the desired areas, the directivity can be further improved with lower interference levels [15]. It is evidently observed that the gain and directivity can be optimized by the number of directors [16, 17]. Also, the length and spacing between the reflector and directors in the Yagi-Uda setup plays a dominant role in the antenna performance [18].

These kinds of antennas are well suitable for source antenna design in beam scanning applications. Realization of wide-angle beam coverage is considered as a huge achievement in the field of modern wireless communication systems. This can be accomplished using integrated lens technique such as Luneburg lens which provides wide angle beam scanning property that is offered by the existence of focal points along the circumference. In [19], the authors introduce a six-layer Luneburg lens integrated with Substrate integrated waveguide (SIW) antenna at 79 GHz for the wide beam scanning in automotive radar application. It provides a maximum gain of 15 dBi and covers 170° beam scan. Several structures of Luneburg lens with array configuration have been reported [20–26] for various applications. The beam steering at 60 GHz using Luneburg lens is depicted in [21] and achieves high gain of 18 dBi. Anyhow, the beam covers only up to 60° of scan angle, and only 9 GHz bandwidth is accomplished. The 2D Luneburg lens presented in [24] varies the refractive index according to change in width after combining meander crossed microstrip line. Luneburg lens can also be designed using PCB process and implemented in W band which involves simple fabrication process [25]. Realization of beam scanning array with Luneburg lens is performed by utilizing the switching units which automatically switches the array element into a predefined beam angle. The printed Yagi-Uda array antenna designed at 300 GHz [27] is investigated and observed, and it can be used as a source antenna for the wide-angle beam scanning. It can be improved by the substrate lens antenna which provides narrow beam directivity. An integrated lens antenna with wide focal points at the circumference after compression provides wide angle beam coverage [28]. This provides only up to 86° scan angle with a bandwidth of 76–81 GHz.

In this work, Luneburg lens is integrated with an array of highly efficient Yagi-Uda substrate lens antenna (SLA) in a semicircular way to obtain a wide-angle beam scanning of 146 degrees around 300 GHz. The maximum realized gain of 17.1 dBi with 83 GHz bandwidth is achieved using the proposed design.

Section 2 shows the primary design of a sub-THz Yagi-Uda antenna with the analysis of gain and bandwidth for different numbers of directors. The Luneburg lens with six layers having different permittivities is designed in Section 3. Section 4 provides beam scanning by placing the SLA towards the circumference of the Luneburg lens. The array of SLA with Luneburg lens provides a high gain of 17.1 dBi and a bandwidth of 82 GHz with a beam coverage of 146°. The results are verified and validated using CST and HFSS simulation software.

2. YAGI-UDA ANTENNA DESIGN

In this section, the design of a Yagi-Uda antenna to maximize the radiation in one direction is presented. Figures 1(a)–(b) illustrate the perspective and front view geometry of the proposed optimized Yagi-Uda antenna, and the analysis of antenna using gain and bandwidth is detailed in this section. The design requirements of the antenna are given in Table 1.

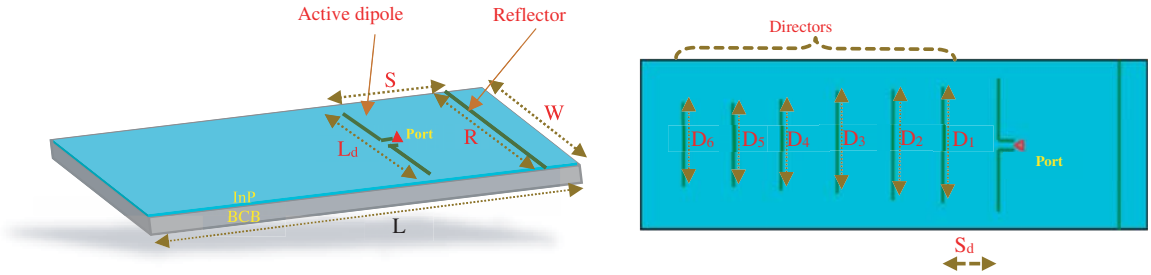

Figure 1. Designed geometry of Yagi-Uda antenna. (a) Perspective view. (b) Top view.

Table 1. Design requirements of Yagi-Uda antenna.

Elements	Length of the elements
Length of the feeding element (L_d)	0.45λ–0.49λ
Length of the reflector (R)	Slightly greater than the feeding element
Spacing between the reflector and the feeding element (S)	Around 0.25λ
Length of directors (D)	0.4λ–0.45λ
Spacing between the directors (SD)	0.3λ–0.4λ

The active dipole element is placed next to the reflector at a distance of $\lambda/4$ in order to enhance directivity and gain in the desired direction where λ is the wavelength corresponding to the designed frequency (300 GHz). The substrate used for the Yagi-Uda design is composed of two layers, and the details of the layers are given in Table 2.

Table 2. The material details used in the design.

Substrate	Permittivity	Height	Loss Tangent
Indium Phosphide (InP)	12.5	6 µm	0.002
Benzocyclobutene (BCB)	2.5	50 µm	0.005

The Yagi-Uda antenna design is printed on a 2 layered substrate in which the bottom layer material Benzocyclobutene (BCB) having dielectric constant of 2.5 with loss tangent of 0.0005 which shows stable behavior over broadband THz frequencies [22]. Both materials having different dielectric constant show very high geometric tolerance up to 350 GHz. The accuracy of the proposed design with the double layered substrate will be high and stable for the frequencies up to 380 GHz.

The metal deposition on the substrate for the active dipole and reflector is designed using gold having a thickness of 2 µm with conductivity of 4.561×10^7 S/m. Figure 2 shows a variation of gain and bandwidth with the number of directors, and it is observed that a significant increase in gain and slight decrease in bandwidth as the number of director increases from one to nine, respectively. It is clearly observed that the maximum gain is achieved for six directors with different lengths. The optimized design geometry of each element of the Yagi-Uda antenna in agreement with the design criteria is given in Table 3. The active dipole element resonates at 300 GHz with maximum gain of 9.12 dBi and also provides a bandwidth of 46 GHz from 294 GHz to 340 GHz as shown in Figure 3. Figures 4(a)–(b) illustrate the 3D radiation pattern showing the gain and directivity of 9.12 dBi and 9.87 dBi, respectively.

Table 3. The optimized dimensions of the Yagi-Uda antenna.

Dimensions	Values
W	300 µm
L	575 µm
R	300 µm
L_d	272 µm
S_d	5 µm
D_1	220 µm
D_2	200 µm
D_3	190 µm
D_4	180 µm
D_5	170 µm
D_6	162 µm

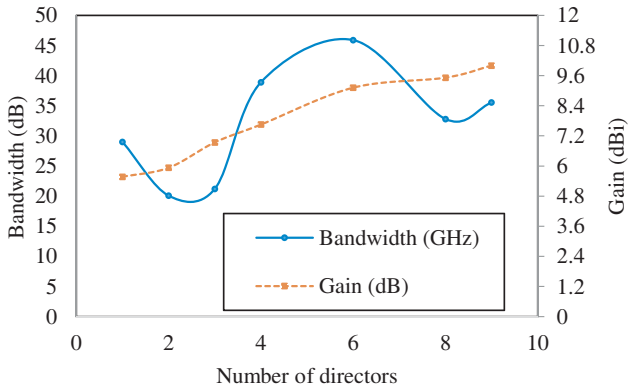

Figure 2. The optimization of gain and bandwidth with different numbers of directors.

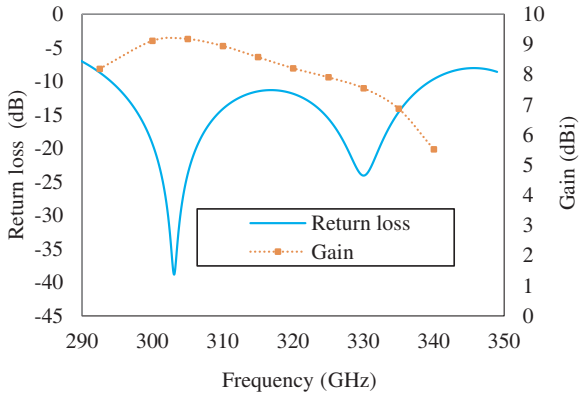

Figure 3. The gain and S parameter analysis of Yagi-Uda antenna in CST suite.

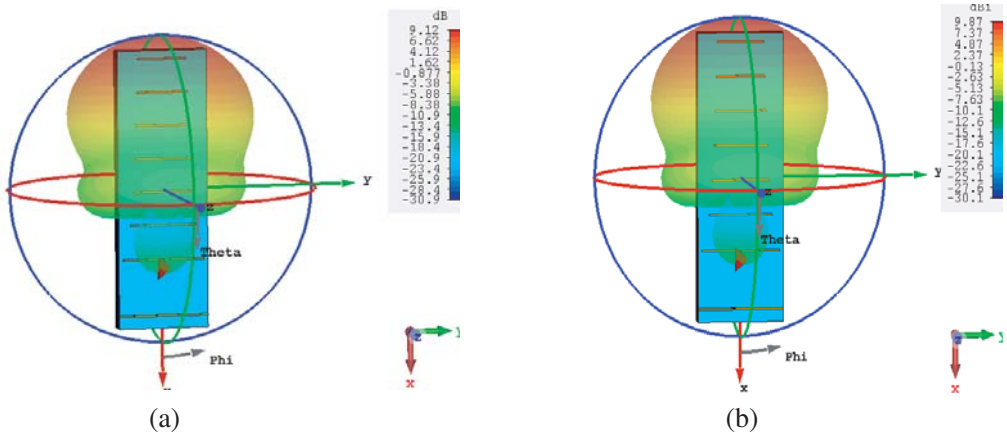

(a) (b)

Figure 4. 3D far-field radiation pattern at 300 GHz. (a) Gain. (b) Directivity.

Further enhancement in the gain and directivity can be obtained with the modification of substrate in the form of a lens, and this technique is discussed in Section 3.

3. SUBSTRATE LENS TECHNIQUE

The two-layer substrates of the Yagi-Uda antenna are modelled, and it is found that the performance of the antenna can be further expanded using substrate lens method. Director axis of the substrate is grated in the shape of a lens and forms SLA, where a part of the substrate which is modeled as SLA is shown in Figure 5(a), and Figure 5(b) shows the perspective view of the proposed SLA.

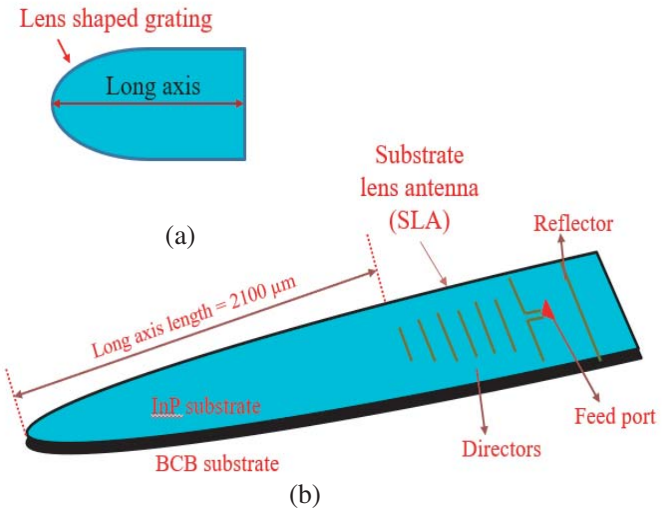

Figure 5. (a) Geometry of the substrate lens (Top view). (b) Perspective view of SLA.

The length of the long axis is optimized, and the simulation output in terms of gain and side lobe level for the frequencies 292 GHz, 300 GHz, and 335 GHz is observed. The variation of gain is shown in Figure 6(a) and found to increase as length of the long axis increases. However, as the long axis length increases, side lobe level rises as observed in Figure 6(b).

The gain of the substrate lens antenna is maximum as the length of the long axis approaches 2400 µm. After considering the side lobe level, the long axis length is optimized to 2100 µm. The

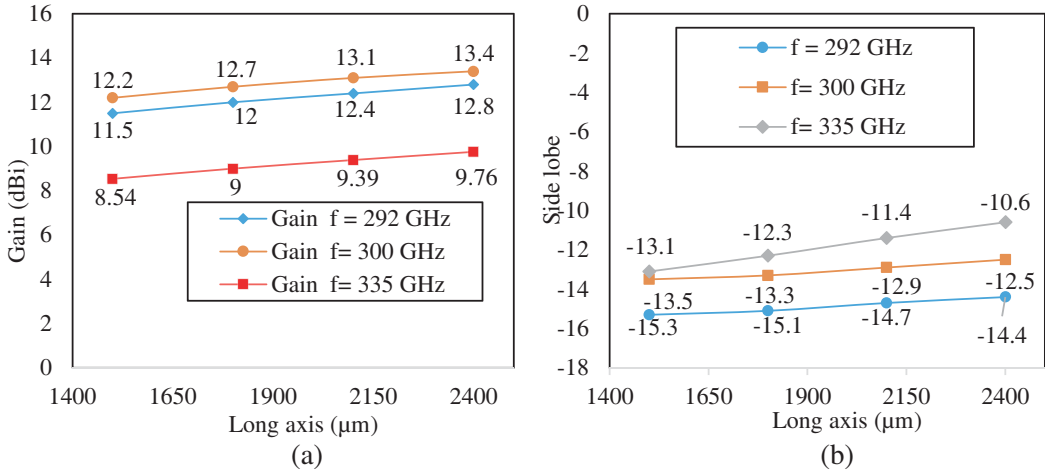

Figure 6. Optimization of long axis length of substrate lens. (a) Gain. (b) Side lobe.

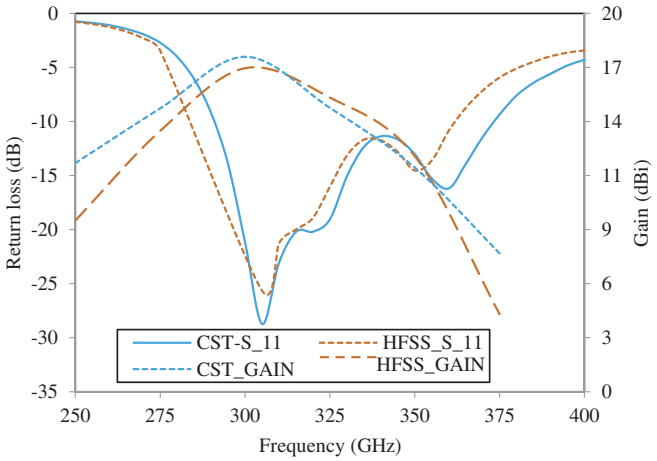

Figure 7. Simulated S parameter and gain plot.

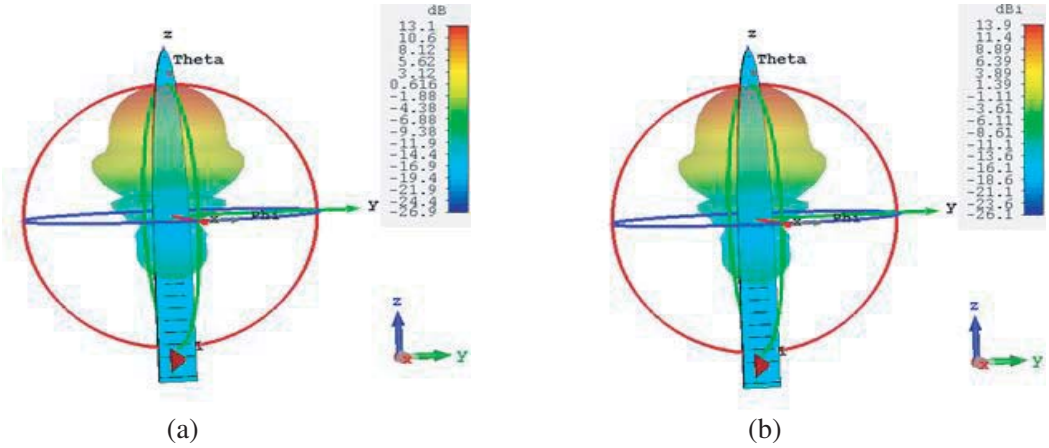

(a) (b)

Figure 8. 3D far-field radiation pattern of substrate lens antenna. (a) Gain. (b) Directivity.

director array elements are arranged vertically along the long axis of the SLA. Figure 7 gives the simulation results for the gain and return loss using this technique which presents 50% increase in bandwidth (292 GHz to 374 GHz).

The SLA provides maximum gain of 13.1 dBi as shown in Figure 8(a), which is 4 dBi greater than single directional Yagi-Uda antenna. The maximum realized gain is also observed from the 3D radiation pattern with 38° beam-width illustrated in Figure 8(a). The antenna is linearly polarized, and end-fire radiation pattern at 300 GHz is observed with a directivity of 13.9 dBi in Figure 8(b).

4. DESIGN OF LUNEBURG LENS

The geometry of inhomogeneous cylindrical Luneburg lens is displayed in Figure 9(a). It is the dielectric gradient index lens which satisfies the specific law (1) that relates the relative permittivity (ε_r) and normalized radius (r) of the luneburg lens whose relative permittivity deviates radially towards the circumference. Its feature of infinite focal point makes it suitable for using for wide beam scanning antenna. The radius and permittivity of each layer inside the lens is designed using Equations (2) and (3).

$$\varepsilon_r = 2 - r^2 \tag{1}$$

$$\varepsilon_i = 2 - (2i - 1)M \tag{2}$$

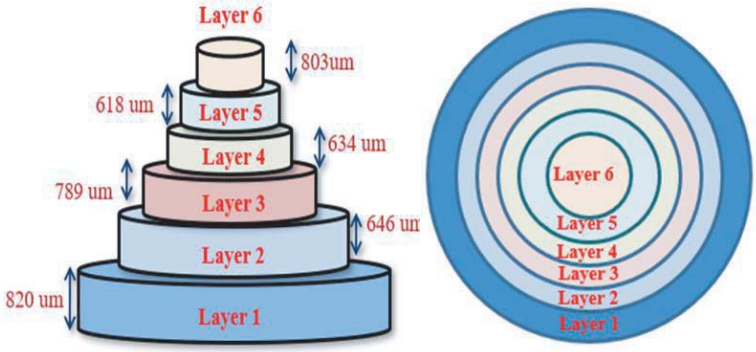

(a) (b)

Figure 9. Structure of Luneburg lens. (a) Side view before compression. (b) Top view after compression.

$$r_i = (2 - \varepsilon_i + M)^{1/2} \tag{3}$$

Six-layer Luneburg lens is designed by using these equations having outer diameter of $3\lambda_0$, where λ_0 is the free space wavelength at frequency of 300 GHz. Thickness of the optimized lens is chosen to be 224 µm. Table 4 shows the height and radius of each layer before compression.

Table 4. The geometry of the Luneburg lens.

	Height of lens (µm)	Outer radius (µm)
Layer-1	820	1140
Layer-2	646	1040
Layer-3	789	931
Layer-4	634	806
Layer-5	618	660
Layer-6	803	465

The basic foam material such as AirexR82 with ε_r 1.12 and thickness 224 µm is utilized for the development of Luneburg lens. To obtain different values of relative permittivity at required areas and to have final thickness of 224 µm, the basic foam material is pressed in a controlled manner at a fixed temperature of 90°C. The air bubbles that are filled inside the foam material are removed at this temperature setup. The dielectric constant of the pressed foam can be controlled in the design by choosing the optimum area density ratio given in Eq. (4),

$$\xi = \frac{H_i}{H_f} \tag{4}$$

where H_i is the initial foam thickness, and H_f is the final foam thickness after compression. The height of all the layers shrinks to 224 µm. The variation of radius and permittivity of each layer is depicted in Table 5. Figure 9(b) illustrates the top view of Luneburg lens after compression.

To achieve the design of the lens with different areas having different thicknesses, cylindrical shaped basic foam material is drilled in a 2D mechanical process, and its dielectric constant and loss tangent are measured in characterization free space measurement setup which consists of AB millimeter VNA and lens horn antennas [17].

Table 5. Final designed Luneburg lens properties for different ε.

$\xi = H_i/H_f$	H_i (mm)	H_f (mm)	Relative permittivity	Loss tangent
8	28	224	1.92	0.015
6.5	22.75	224	1.77	0.014
5.35	18.725	224	1.62	0.013
4.2	14.7	224	1.46	0.01
2.75	9.625	224	1.31	0.008
1.5	5.25	224	1.15	0.007

5. PROPOSED 9 ELEMENT SLA ARRAY WITH LUNEBURG LENS

Figure 10 shows the single SLA integrated with Luneburg lens at its circumference to obtain an increase in the gain of 4.7 dBi compared to single source antenna. The maximum gain of 17.7 dBi with a bandwidth of 82 GHz (from 291 GHz to 373 GHz) at the center frequency of 300 GHz is observed from Figure 11(a) and verified using HFSS. The simulated 2D co-polar radiation pattern of single SLA with Luneburg lens in CST microwave studio suite is observed in Figure 11(b) which shows narrow beamwidth of 17.3°, and the result is verified using commercially available electromagnetic simulation software HFSS due to the lack of fabrication and measurement facility at the simulated laboratory. The similarity between the simulated co-polar radiation patterns on two different algorithms in Figure 11(b) are validated by using the feature selective validation (FSV) tool [29–31], and feature difference measure (FDM) chart [31] is shown in Figure 11(c). The good and fairly similar results from both software raise the accuracy level of measurement outcome. The maximum gain is obtained at 0° beam shift and possesses minimum side lobe level of −15.94 dBi.

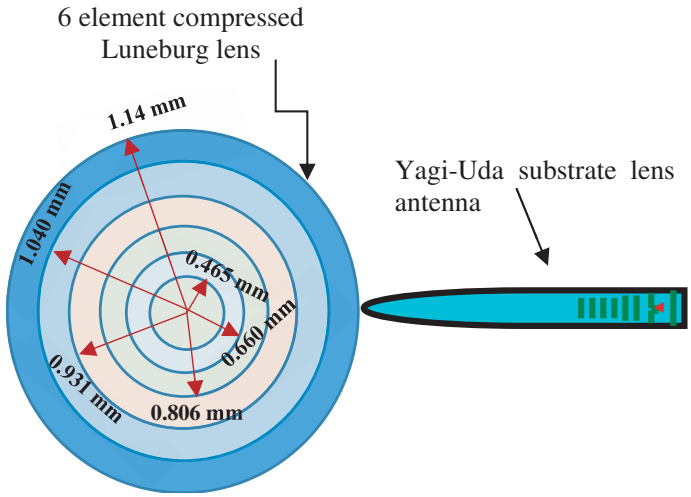

Figure 10. The single substrate lens Yagi-Uda antenna integrated with Luneburg lens.

The array of SLA is integrated with Luneburg lens as shown in Figure 12 in order to achieve beam scanning. Utilizing the existence of several focusing points at the circumference of the Luneburg lens, the final antenna achieves a wide-angle beam scanning in the azimuth plane. The simulated matched return loss with maximum bandwidth of 83 GHz which ranges from 289 GHz to 372 GHz at 300 GHz center frequency is shown in Figure 13(a). The 2D co-polar far-field radiation pattern of the final structure with one SLA illuminated at a time is illustrated in Figure 13(b), and the simulation results are verified using HFSS software. The spacing between the SLA and Luneburg lens is optimized to

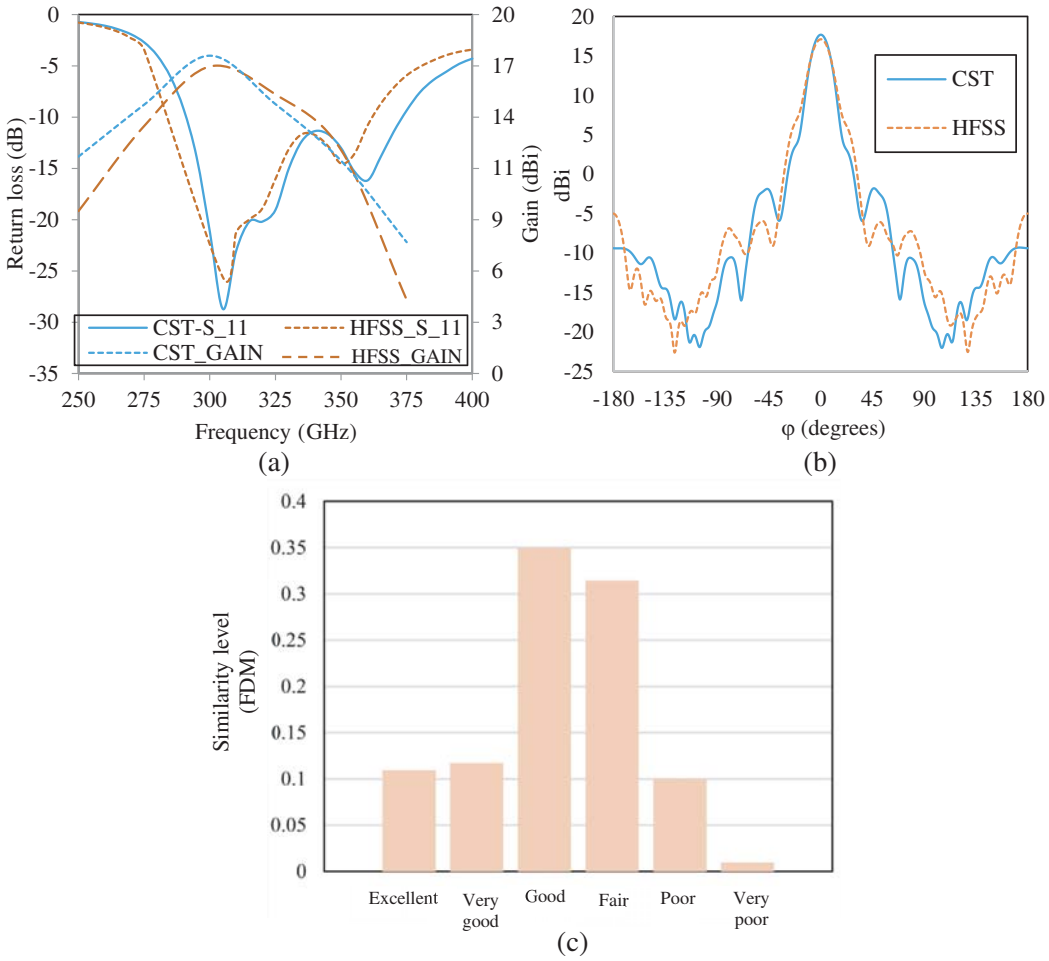

Figure 11. (a) Analysis of simulated Gain and return loss. (b) Co-Polar radiation pattern of single element Luneburg lens at 300 GHz. (c) Result validation using FSV tool.

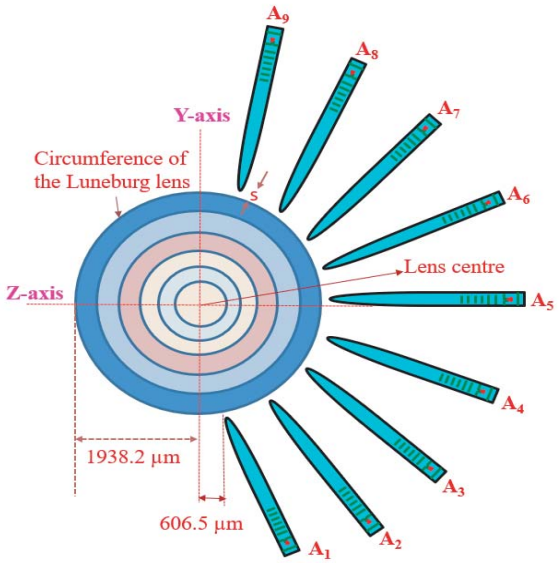

Figure 12. The final 9 element array integrated with Luneburg lens.

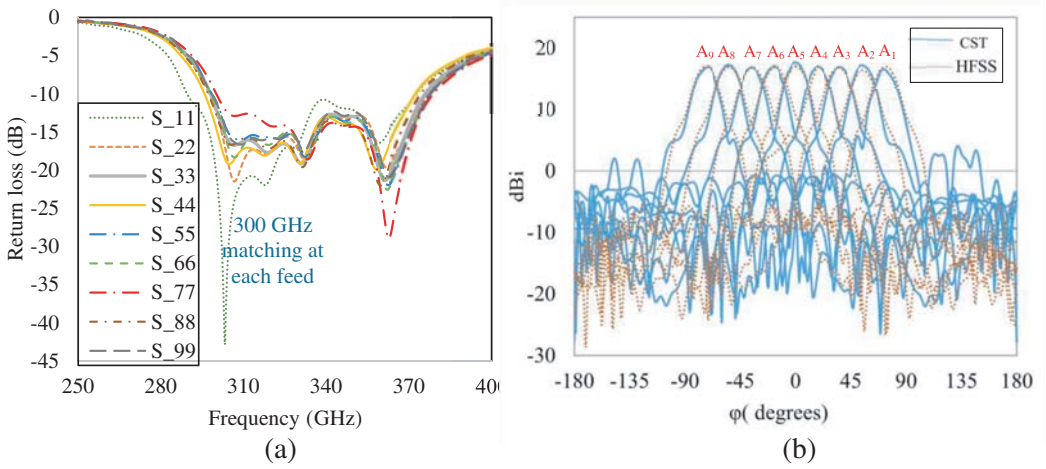

Figure 13. (a) Simulated matched return loss of Final 9-array Yagi-Uda antenna with Luneburg lens illuminating one Yagi antenna at a time. (b) Verification of co-polar beam scanning radiation pattern using CST and HFSS at 300 GHz.

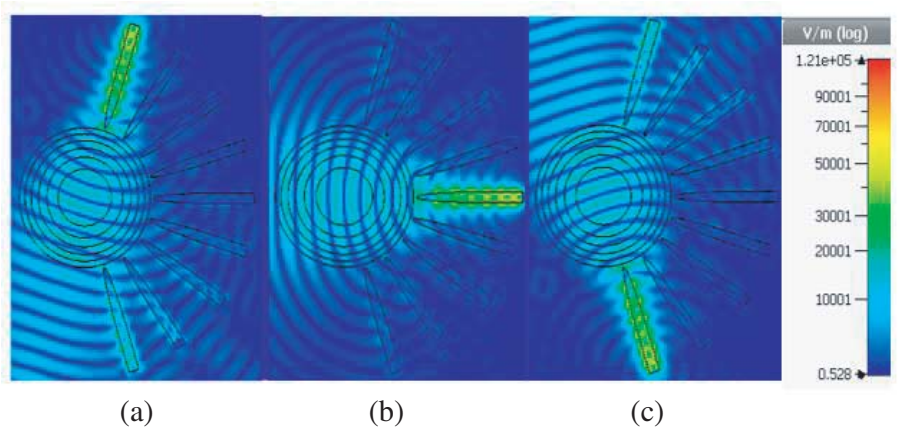

Figure 14. *E*-field distribution. (a) A_9 is energized. (b) A_5 is energized. (c) A_1 is energized.

72 µm and possesses tolerable geometric spacing from 72 µm to 92 µm without adverse effect in the reflection and radiation characteristics.

Each element in the SLA array is denoted by A_1, A_2, A_3, A_4, A_5, A_6, A_7, A_8, and A_9 with center SLA as A_5. The nine SLA elements are excited separately, and center SLA element provides a radiation pattern without any deviation from $\varphi = 0°$. The elements at the edges represented by A_1 and A_9 have a beam shift of $+73°$ and $-73°$, respectively. Thereby, the proposed antenna using the 9-element array setup has a wide beam coverage of 146° with a maximum gain of 17.2 dBi observed between the feed ports at A_1 to A_9. The array elements A_1, A_2, A_3, and A_4 provide the maximum gain towards the angles 73°, 55°, 35°, and 17.2°, respectively. Thus, the beam can cover up to 73° towards the positive scan angle using the 4-element array with a beamwidth of 17.3°.

Similarly, maximum radiation is obtained at 17.2°, 35°, 55°, and 73° when exciting the array elements A_6, A_7, A_8, and A_9, respectively. The electric field distribution pattern (at 300 GHz) of the array antenna where 3 elements at A_1, A_5, and A_9 are excited, and others are terminated by 50 Ω load is shown in Figures 14(a)–(c).

Maximum gain is obtained when the center source element (i.e., A_5) is energized as in Figure 14(b), and minimum gain is obtained when the elements at the edges such as A1 and A9 are energized. The gain reduction is due to the encounter of radiation from the SLA at the two edge feeds. The total

Table 6. The augmented results of the proposed work with respect to the results obtained from similar literatures at frequencies beyond 50 GHz.

Reference	Work Type	Maximum Gain (dBi)	Bandwidth (GHz)	Maximum efficiency	Beam scanning coverage
[3]	Array	1.72	6.07	ng	na
[16]	Single	12.9	0.3 T	77.7	na
[19]	Array	15	7.5	67	$+/-85^\circ$
[21]	Lens	18	9	ng	$+/-30^\circ$
[22]	Array	13.6	82	89	na
[28]	Lens network	12.3	1.6	63	$+/-41$
This work	Lens array	17.2	83	92.9	$+/-73$

ng: not given
na: not applicable

radiation efficiency is estimated as 92.9% at 300 GHz.

Table 6 shows the qualitative comparison between the proposed work and other similar works which exhibit the wide beam-scan coverage along with improved bandwidth and gain over the sub-THz range.

6. CONCLUSION

This work presents a Yagi-Uda substrate lens antenna which is integrated with Luneburg lens in order to generate beam scanning at 300 GHz for sub-THz applications. The cylindrical Luneburg lens having several focal points along the circumference is utilized for beam scanning. The Yagi-Uda substrate lens antenna is used for a source array, and the setup gives the bandwidth of 83 GHz (289 GHz to 372 GHz) at 300 GHz center frequency. The beamwidth of 17.3° is achieved using the 9-element array, and the maximum gain perceived between the elements A_1 to A_9 is 17.2 dBi. The front to back ratio is 14 dBi. From Figure 13(b) of beam scanning, it is clear that beam is scanned between -73° and $+73^\circ$ which is provided by each array element from A_1 to A_9. The overall coverage of 146° at 300 GHz is achieved which has a wide range of telecommunication and radar applications. The proposed antenna limits the complications emerging when the beam scanning antennas are designed at 300 GHz such as high path loss, attenuation by objects, and misalignment of antennas, and thereby this can be effectively used as a steerable beam antenna for THz applications.

REFERENCES

1. Liu, D., W. Hong, T. S. Rappaport, C. Luxey, and W. Hong, "What will 5G antennas and propagation be?" *IEEE Transactions on Antennas and Propagation*, Vol. 65, No. 12, 6205–6212, 2017.
2. Malhotra, I., K. R. Jha, and G. Singh, "Terahertz antenna technology for imaging applications: A technical review," *International Journal of Microwave and Wireless Technologies*, Vol. 10, No. 3, 271–290, 2018.
3. Guo, L., M. Deng, Q. Zhang, X. Zhang, and Z. Yuan, "Dual-polarized on-chip antenna for 300 GHz full-duplex communication system," *International Journal of Antennas and Propagation*, Vol. 2017, Article ID 2837629, 7 pages, 2017.
4. Balanis, C. A., *Antenna Theory: Analysis and Design*, 4th Edition, Wiley Publishers, Hoboken, NJ, USA, 2017.

5. Ismail, M. Y. and N. H. Sulaiman, "Enhanced bandwidth reflectarray antenna using variable dual gap," *International Conference on Instrumentation, Communication, Information Technology and Biomedical Engineering*, IEEE, Bandung, Indonesia, 2011.
6. Florencio, R., R. R. Boix, and J. A. Encinar, "Design of a reflectarray antenna at 300 GHz based on cells with three coplanar dipoles," *2013 IEEE Antennas and Propagation Society International Symposium (APSURSI)*, IEEE, 2013.
7. Muñoz-Acevedo, A., M. Sierra-Castañer, and J. L. Besada, "Antenna measurement system at 300 GHz for the terasense project," *Proceedings of the Fourth European Conference on Antennas and Propagation*, 1–5, 2010.
8. Rey, S., T. Merkle, A. Tessmann, and T. Kürner, "A phased array antenna with horn elements for 300 GHz communications," *Proceedings of ISAP-2016*, 122–123, IEEE, Okinawa, Japan, 2016.
9. Azizi, M. K., M. A. Ksiksi, H. Ajlani, and A. Gharsallah, "Terahertz graphene-based reconfigurable patch antenna," *Progress In Electromagnetics Research Letters*, Vol. 71, 69–76, 2017.
10. Chen, J., K. Yuan, L. Shen, X. Deng, L. Hong, and M. Yao, "Studies of terahertz wave propagation in realistic reentry plasma sheath," *Progress In Electromagnetics Research*, Vol. 157, 21–29, 2016.
11. Priebe, S., C. Jastrow, M. Jacob, T. Kleine-Ostmann, T. Schrader, and T. Kürner, "Channel and propagation measurements at 300 GHz," *IEEE Transactions on Antennas and Propagation*, Vol. 59, No. 5, May 2011.
12. Bankey, V. and N. Anvesh Kumar, "Design of a Yagi-Uda antenna with gain and bandwidth enhancement for Wi-Fi and Wi-Max applications," *International Journal of Antennas (JANT)*, Vol. 2, No. 1, 1–14, January 2016.
13. Cai, R.-N., Y. Chuan, L. Shu, X.-Q. Zhang, X.-Y. Zhang, and X.-F. Liu, "Design and analysis of printed Yagi-Uda antenna and two-element array for WLAN applications," *International Journal of Antennas and Propagation*, Article Id 651789, 8 Pages, 2012.
14. Han, K., T. K. Nguyen, and I. Park, "Yagi-Uda antenna with U-shaped dipole for a THz photomixer," *34th International Conference on Infrared, Millimeter, and Terahertz Waves*, 2009.
15. Mathew, P. K., "A three element Yagi Uda antenna for RFID systems," *IJEDR*, Vol. 2, No. 1, ISSN: 2321–9939, 2014.
16. Sethi, W. T., O. De Sagazan, H. Vettikalladi, H. Fathallah, and M. Himdi, "Yagi-Uda nantenna for 1550 nanometers optical communication systems," *International Journal of Antennas and Propagation*, Vol. 60, No. 9, 2236–2242, 2018.
17. Sharma, Y. and S. Nagpal, "Radiation pattern optimization of a 6 element Yagi-Uda antenna," *IJREST International Journal of Research Review In Engineering Science & Technology*, Vol. 5, No. 1, Issn 2278–6643, 2016.
18. Prasada Reddy, M., "Directional Yagi Uda antenna for VHF applications," *International Journal of Advancements in Technology*, Vol. 9, No. 3, Issn: 0976–4860, 2018.
19. Kamran Saleem, M., H. Vettikaladi, M. A. S. Alkanhal, and M. Himdi, "Lens antenna for wide angle beam scanning at 79 GHz for automotive short range radar applications," *IEEE Transactions on Antennas and Propagation*, Vol. 65, No. 4, 2041–2046, Apr. 2017.
20. Rondineau, S., M. Himdi, and J. Sorieux, "A sliced spherical Luneburg lens," *IEEE Antennas and Wireless Propagation Letters*, Vol. 2, 163–166, 2003.
21. Foster, R., D. Nagarkoti, J. Gao, B. Vial, F. Nicholls, C. Spooner, S. Haq, and Y. Hao, "Beam-steering performance of flat Luneburg lens at 60 GHz for future wireless communications," *International Journal of Antennas and Propagation*, Article Id 7932434, 8 pages, 2017.
22. Vettikalladi, H., W. T. Sethi, A. F. Bin Abas, W. Ko, M. A. Alkanhal, and M. Himdi, "Sub-THz antenna for high-speed wireless communication systems," *International Journal of Antennas and Propagation*, Article ID 9573647, 9 pages, 2019.
23. Knyazev, S., A. Korotkov, B. Panchenko, and S. Shabunin, "Investigation of spherical and cylindrical Luneburg lens antennas by the Green's function method," *IEEE Radio and Antenna Days of the Indian Ocean*, IEEE Radio, 2015.

24. Zhou, B., Y. Yang, H. Li, and T. J. Cui, "Beam-steering Vivaldi antenna based on partial Luneburg lens constructed with composite materials," *Journal of Applied Physics*, Vol. 110, 084908, 2011.
25. Chen, H., Q. Cheng, A. Huang, J. Dai, H. Lu, J. Zhao, H. Ma, W. Jiang, and T. J. Cui, "Modified Luneburg lens based on metamaterials," *International Journal of Antennas and Propagation*, Article Id 902634, 6 pages, 2015.
26. Liang, M., W.-R. Ng, K. Chang, K. Gbele, M. E. Gehm, and H. Xin, "A 3-D Luneburg lens antenna fabricated by polymer jetting rapid prototyping," *IEEE Transactions on Antennas and Propagation*, Vol. 62, No. 4, 1799–1807, 2014.
27. Pfeiffer, C. and A. Grbic, "A printed, broadband Luneburg lens antenna," *IEEE Transactions on Antennas and Propagation*, Vol. 58, No. 9, 3055–3059, 2010.
28. Numan, A. B., J.-F. Frigon, and J.-J. Laurin, "Printed W-band multibeam antenna with Luneburg lens-based beamforming network," *IEEE Transactions on Antennas and Propagation*, Vol. 66, No. 10, 5614–5619, 2018.
29. IEEE Standard P1597, "Standard for validation of computational electromagnetics computer modeling and simulation — Part 1, 2," 2008.
30. Duffy, A. P., A. J. M. Martin, A. Orlandi, G. Antonini, T. M. Benson, and M. S. Woolfson, "Feature selective validation (FSV) for validation of computational electromagnetics (CEM). Part I — The FSV method," *IEEE Trans. on Electromagn. Compatibility*, Vol. 48, No. 3, 449–459, Aug. 2006.
31. Orlandi, A., A. P. Duffy, B. Archambeault, G. Antonini, D. E. Coleby, and S. Connor, "Feature selective validation (FSV) for validation of computational electromagnetics (CEM). Part II — Assessment of FSV performance," *IEEE Trans. on Electromagn. Compatibility*, Vol. 48, No. 3, 460–467, Aug. 2006.